JACS
JOURNAL OF THE AMERICAN CHEMICAL SOCIETY

Article

pubs.acs.org/JACS

Stochastic Gate Dynamics Regulate the Catalytic Activity of Ubiquitination Enzymes

Manoj K. Rout,[†] Curtis D. Hodge,[†] Craig J. Markin,[†] Xin Xu,[‡] J. N. Mark Glover,[†] Wei Xiao,[‡,§] and Leo Spyracopoulos*[,†]

[†]Department of Biochemistry, University of Alberta, Edmonton, Alberta T6G 2H7, Canada

[‡]College of Life Sciences, Capital Normal University, Beijing 100048, China

[§]Department of Microbiology and Immunology, University of Saskatchewan, Saskatoon, Saskatchewan S7N 5E5, Canada

Supporting Information

ABSTRACT: Initiation of the DNA damage and innate immune responses is dependent upon the flow of chemical information through coupled protein−protein interaction networks and driven by the synthesis and recognition of Lys 63 linked polyubiquitin (polyUb) chains on adaptor proteins. The central chemical step in Lys 63-linked protein ubiquitination involves the reaction of a specific lysine on a target protein with Ub that is covalently attached as a thioester conjugate to the Ub conjugating enzyme (E2) Ubc13. The active site cysteine of Ubc13, and E2 enzymes in general, is buttressed by a flexible loop. The role of loop dynamics in catalysis was investigated by mutating the central and hinge residues to glycine. The loop dynamics were experimentally characterized through measurement of enzyme kinetics, main chain NMR relaxation, X-ray crystallographic studies, and in vivo studies in yeast. The experimental data were complemented by analysis of MD simulations of the dynamics and kinetics for the loop motion. The results show that fast pico- to nanosecond time scale active site loop fluctuations play a crucial role in regulating the catalytic activity of Ubc13 by functioning as a stochastic active site gate, which is characterized by precisely balanced rates of opening and closing. In vivo functional complementation assays in yeast demonstrate that defects within this regulatory mechanism can have profound biological consequences, given that Ubc13 is the only E2 dedicated to synthesizing Lys 63-linked polyUb chains.

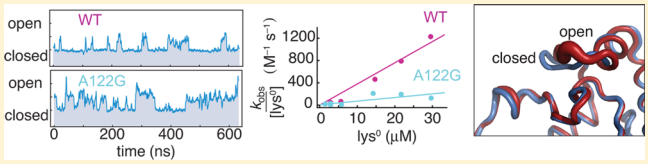

INTRODUCTION

A hallmark of life processes is the flux of chemical information through coupled protein−protein interaction networks, initiating, for example, DNA damage and innate immune responses,[1,2] through the synthesis and recognition of polyubiquitin (polyUb) chains on adaptor proteins.[3,4] Protein ubiquitination involves the sequential catalytic activity of three enzymes, beginning with covalent attachment of the C-terminus of Ub to the active site cysteine of a Ub activating enzyme (E1), a subsequent transfer as a thioester conjugate to a Ub conjugating enzyme (Ubc∼Ub or E2∼Ub), and terminating with attachment of Ub to a target protein through the activity of a ubiquitin ligase (E3), which binds both E2 and target.[5,6] This final nucleophilic acyl substitution is characterized by the attack of a specific target lysine on the thioester bond to yield a stable Ub−protein target amide bond. The coupled activity of the ubiquitination enzymes to downstream protein−protein interaction cascades implies that a modest change in any of the associated kinetics, whether chemical steps or binding, will give rise to defects in signal transmission with serious consequences for the ability of cells to thrive and maintain homeostasis. However, the molecular mechanisms underlying ubiquitination, particularly the coupling of structure and dynamics, and their role in the catalytic activity for the central E2 enzyme remain to be resolved.

E2 ubiquitin conjugating enzymes play a central role in the ubiquitination cycle by bridging ATP-dependent activation of the C-terminus of Ub and its ultimate transfer to a target protein.[7,8] The fundamental E2 protein fold, consisting of ∼150 residues, has evolved mainly to achieve a large rate enhancement, in excess of 10^6-fold,[9] for nucleophilic attack of lysine on the C-terminus of Ub, which is attached to the E2 through a thioester bond. Interestingly, a veil of regulatory control involving weak binding of substrates and cofactors provides a relatively small, ∼1000-fold increase in catalytic rate for E2 enzymes, which is essential for biological specificity.[9−13] Further, E2 enzymes orchestrate diverse functions, including controlling the shift from initiating Ub chain synthesis on targets to chain elongation, selecting the specific lysine through which Ub monomers are sequentially linked, as well as regulating the timing of chain release during elongation.[8]

The active site of E2 enzymes is composed of a C-terminal region that buttresses the catalytic cysteine with a flexible loop.[14,15] In order to illuminate the role of the loop dynamics in the catalytic activity of E2 enzymes, we hypothesized that the conformational fluctuations of the loop from the E2 Ubc13 function as a stochastic gate to regulate catalytic activity.

Received: November 28, 2013
Published: November 25, 2014

dx.doi.org/10.1021/ja505440b | J. Am. Chem. Soc. 2014, 136, 17446−17458

Among family members, Ubc13 is unique in that it is the only E2 dedicated to catalyzing the synthesis of polyUb chains linked through lysine-63 as a result of its interaction with the Ub-binding Ubc enzyme variant (UEV) Mms2.[16] To investigate the role of enzyme dynamics in catalysis, we mutated three loop residues to glycine, the amino acid with the least conformational restriction. Two mutations were located near the loop hinge points (D118G, A122G), and one in the center of the loop (L121G). The gating mechanism was experimentally characterized through measurements of enzyme kinetics, main chain ^{15}N NMR relaxation, X-ray crystallographic studies, and in vivo functional complementation studies in yeast. A detailed atomic view of the gate motion was obtained with molecular dynamics (MD) simulations for free Ubc13, as well as Ubc13 conjugated to Ub through a thioester bond. In addition to studies involving the D118G, L121G, and A122G mutants, the role of active site desolvation was examined through enzyme kinetics measurements for the central loop residue mutants L121A, L121V, and L121I. Blending experimental studies with simulations demonstrates that stochastic, nanosecond time scale gate fluctuations regulate the catalytic activity of ubiquitin conjugation enzymes.

EXPERIMENTAL SECTION

Cloning, Expression, and Purification of Ubc13 and Mutants. Human Ubc13 was cloned into the pHis-P1 plasmid. In order to examine the role of dynamics in catalysis, Ubc13-D118G, Ubc13-L121G, and Ubc13-A122G were generated by site-directed mutagenesis using a QuikChange mutagenesis kit. To test the role of active site desolvation in catalysis, Ubc13-L121A, L121V, and L121I were also generated using site-directed mutagenesis. [*U*-^{15}N]- and [*U*-^{15}N,^{13}C]-Ubc13 D118G, L121G, and A122G constructs were expressed in *Escherichia coli* strain BL21(DE3)-RIPL according to the protocol described by Bracken and co-workers,[17] with additional details as previously reported.[18,19] Harvested cells were suspended in ∼100 mL of lysis buffer containing 500 mM NaCl, 20 mM sodium phosphate, 100 μg/mL DNase I, 1 mM DTT, 10 mM $MgSO_4$, and 0.5% protease inhibitor cocktail II (Calbiochem catalog no. 538132). Cells were lysed by sonication, and the lysate was centrifuged at 25 000 rpm in a Beckman JA-25.5 rotor for 30 min. The supernatant was then filtered through a Millipore steriflip 0.45 μm vacuum filtration unit. The filtered lysate was loaded onto a His-prep FF16/10 column that was pre-equilibrated in binding buffer (500 mM NaCl, 20 mM sodium phosphate, 20 mM imidazole and 1 mM DTT at pH 7.4) with an AKTA-prime FPLC. His-tagged Ubc13 was eluted from the column with elution buffer (500 mM NaCl, 20 mM sodium phosphate, 500 mM imidazole and 1 mM DTT at pH 7.4). Fractions containing protein were collected, and 100 μL of 210 μM Tev-protease was added. This mixture was dialyzed against 2 L of 150 mM NaCl, 20 mM sodium phosphate and 1 mM DTT at pH 7.4 for 20 h at room temperature using a dialysis membrane with a 3.5 kDa cutoff. The histidine affinity tag was separated from Ubc13 using a His-prep FF16/20 column. Fractions containing protein were concentrated and loaded onto a HiLoad 26/60 Superdex 75 column equilibrated with 150 mM NaCl, 20 mM sodium phosphate and 1 mM DTT at pH 7.4. Peak fractions containing Ubc13 were collected and concentrated to ∼1 mM for the various NMR samples. For enzyme assays and X-ray crystallography, wild type Ubc13 and the various mutants were expressed in LB instead of M9 media, with the same purification protocol described above.

Crystallization and X-ray Crystallography. Ubc13-D118G, L121G, and A122G mutants were added to purified Mms2 to form a heterodimeric complex. The complex was further purified and exchanged by gel filtration into buffer containing 50 mM HEPES, 75 mM NaCl, 0.5 mM DTT, pH 7.5. The complex was concentrated to 6 mg/mL for crystallization. Crystals were grown using vapor diffusion. Initial Ubc13-L121G and Ubc13-D118G hits were in 0.1 M sodium citrate pH 6.8, 20% PEG 8000. Crystals were crushed to make seed stocks in the mother liquor. A 1/100 000 dilution of the seed stocks in 0.1 M sodium citrate pH 6.8, 15% PEG 8000 was performed in serial steps of 1/10. A cat whisker was used to streak microcrystals from the diluted crystal solution into a crystallization drop that had been pre-equilibrated for 2 h in the dilution solution. The initial Ubc13-A122G hit was in 0.1 M sodium citrate, pH 5.9, 25% PEG 8000. As in the case of Ubc13-L121G and Ubc13-D118G, crystals for Ubc13-A122G were crushed to make a seed stock in the mother liquor, and diluted as described above using a solution of 0.1 M sodium citrate, pH 5.9, 15% PEG 8000. Crystals were cryoprotected through the addition of 25% glycerol and flash frozen in liquid nitrogen. Data were collected on a home-source R-AXIS beamline. The three structures were solved using rigid body refinements in PHENIX of the Ubc13/Mms2 crystal structure[15] (PDB ID code 1J7D) against the mutant data sets.[20] To facilitate comparison between wild type protein and mutants, as well as MD-derived values, per-residue *B*-factors were normalized according to[21]

$$B_{N,i} = (B_i - \langle B \rangle)/\sigma_B \quad (1)$$

where $B_{N,i}$ is the normalized *B*-factor for residue *i*, $\langle B \rangle$ is the mean *B*-factor for all residues with associated standard deviation σ_B. The first and last ∼5 terminal residues were excluded from the calculation. This approach has the advantage that per residue normalized *B*-factors are given in units of σ_B from a mean of zero.

NMR Spectroscopy: Unconjugated Ubc13 E2 Enzyme and Mutants. NMR spectra for wild type Ubc13, and the D118G, L121G, and A122G mutants were obtained at 25 °C using a Varian Unity INOVA 600 MHz NMR spectrometer. 300 μL samples of [*U*-^{13}C,^{15}N]-Ubc13 and [*U*-^{15}N]-Ubc13 were used for assignment and NMR relaxation experiments (using SHIGEMI microcell NMR tubes), and contained 9:1 H_2O/D_2O with 50 mM phosphate (pH 7.5), 150 mM NaCl for Ubc13, 1 mM DTT, 1 mM DSS, 3 μL of 100× stock protease inhibitor cocktail I for hUbc13 (Calbiochem). For [*U*-^{15}N]-Ubc13 and stochastic gate mutants (D118G, L121G, A122G), ^{15}N-R_1, ^{15}N-R_2, and {^{1}H}-^{15}N NOE experiments were conducted using sensitivity enhanced pulse sequences.[22] ^{15}N-R_1 data were acquired using relaxation delays of 55.5, 122.1, 199.1, 299.7, 399.6, 499.5, 710.4, 804.75, 1010.1 ms. ^{15}N-R_2 data were acquired using relaxation delays of 10, 30, 50, 70, 90, and 110 ms, with a delay between transients of 3.0 s to reduce the effects of sample heating. For {^{1}H}-^{15}N NOE measurements, the spectrum recorded without proton saturation was acquired with a delay between transients of 8 s, whereas the spectrum recorded with proton saturation incorporated a relaxation delay of 5 s, followed by 3 s of proton saturation for a total delay of 8 s. The overall correlation times (τ_c) for wild type Ubc13 and the various stochastic gate mutants were calculated from the R_2/R_1 ratio as previously described.[23,24] Chemical shift changes between mutants and wild type Ubc13 were calculated according to $\Delta\delta = ((\Delta\delta^1H^N)^2 + (\Delta\delta^{15}N/5)^2)^{1/2}$.

Molecular Dynamics Simulations: Unconjugated Ubc13 E2 Enzyme and Mutants. Simulations for wild type Ubc13 and the D118G, L121G, and A122G mutants were conducted using the AMBER 11 or 12 suite of programs,[25] with the *ff*99SBNMR force field[26] and the TIP3P water model. Covalent bonds to hydrogen were restrained using SHAKE, temperature was regulated using Langevin dynamics with a collision frequency of 1 ps^{-1}, and the cutoff was 8 Å for pairwise nonbonded and electrostatic interactions. A particle mesh Ewald approach with default parameters was used for calculating long-range electrostatics. The initial structural models for Ubc13 and the various stochastic gate mutants were solvated in a truncated octahedral water box with a minimum of 24 Å between protein atoms and their images in adjacent unit cells, and neutralized with Na^+ ions to ensure system neutrality. The system was heated over 50 ps to 298 K with 2 kcal/mol restraints on solute atoms, and equilibrated to 1 atm pressure for an additional 50 ps. Production dynamics were then conducted for ∼630−720 ns. A second MD simulation (650 ns) for Ubc13 D118G was conducted in a similar fashion as described above, with the exception that the CUDA implementation of PMEMD[27] and a Berensden thermostat were employed.

Correlation functions for main chain amide $^{15}N-^{1}H^{N}$ vectors were calculated from 16 ns windows corresponding to either the closed or open states for the stochastic gate. The correlation functions for the two states were fit to five parameter multiexponential decays to extract correlation times and subsequently used with experimentally determined τ_c values and five parameter spectral density functions to calculate ^{15}N-R_1, R_2, and NOE values at 600 MHz as previously described.[28] The ^{15}N-R_1, R_2, and NOE values were weighted according to fractions of open and closed state over the ∼600 ns length of the simulations, for example, $R_1 = f_c R_{1,closed} + f_o R_{1,open}$, where f_c and f_o are the fractions closed and open, respectively. This approach was adopted given that the correlation functions for the loop residues generally decay within the lifetimes of the open and closed states. Thus, it is a reasonable approximation to use population weighted relaxation rates rather than a more complicated two state jump model for the correlation functions (Supporting Information, Figure S1). For residue 122, the most flexible residue within the loop, the RMSDs with respect to the experimental relaxation parameters for the closed, open and weighted MD values are WT: 4.1, 2.4, and 3.7, respectively, L121G: 5.5, 5.6, and 5.6, respectively, A122G: 6.0, 5.8, 1.8, respectively, D118G: 3.3, 10.4, and 2.3, respectively. Representative MD-derived ^{15}N-R_1, R_2, and NOE values for the active site loop are shown in Figure S2.

The kinetics of opening and closing for the gate were calculated by analysis of the stochastic fluctuations of the distance between the center of mass for residues 119−121 of the gating loop and residues 87−89 of the active site. The distance was assigned a value of 1 (open state) when it exceeded 8.5 Å, and a value of zero (closed state) below 8.5 Å. The number of open or closed transitions divided by the total time in the open or closed state, respectively, gives the rate of opening or closing.

B-factors were calculated using 16 ns windows from the trajectory corresponding to the closed state of wild type Ubc13 and the L121G mutant. For D118G and A122G, the *B*-factors were calculated using 16 ns windows from trajectory corresponding to the open state. *B*-factors were normalized as described above.

Molecular Dynamics Simulations: E2 Enzymes Conjugated to Ubiquitin through a Thioester Bond. A molecular model for wild type Ubc13 with the active site cysteine ligated to the C-terminus of Ub was generated as previously described,[19] and assumed to adopt a catalytically "active" conformation wherein the C-terminus of Ub lies sandwiched between the loop containing the active site cysteine, and the loop containing L121, as described in recent crystallographic structures.[13] Simulations for wild type Ubc13 and the D118G, L121G, and A122G mutants ligated to Ub through a thioester bond were conducted as described above, with the CUDA implementation of PMEMD. Simulations were conducted in duplicate, once with temperature regulated using a Berensden thermostat, and a second run with temperature regulated using Langevin dynamics, with the exception that simulations for D118G-Ubc13∼Ub in the closed and catalytically competent state were conducted in triplicate, twice using Langevin dynamics and once using a Berensden thermostat. Production dynamics were conducted for ∼700 ns. The opening and closing kinetics for the gate were calculated by analyzing the stochastic fluctuations of the distance between the center of mass for the main chain N, Cα, C′ atoms from residues 121 and 122 of the gating loop and residue 87 in the active site. The distance was assigned a value of 1 (open state) when it exceeded 11 Å, and a value of zero (closed state) below 11 Å. This cutoff value differs from free Ubc13 as a result of the fact that when the C-terminus of Ub lies between the gating loop, and the loop containing the active site cysteine in closed and catalytically active Ubc13∼Ub, the two loops spread apart. As described above, the number of open or closed transitions divided by the total time in the open or closed state, respectively, gives the rate of opening or closing. In a similar fashion, the rates of hydrogen bond formation and cleavage between the side chain amide of N79 from the active site, and the thioester carbonyl were calculated; when the distance between the side chain nitrogen and carbonyl oxygen was <4 Å, the atoms were considered bonded, and when the distance was >4 Å, they were considered not bonded.

In addition to the catalytically active conformation of Ubc13 conjugated to Ub through a thioester bond (Ubc13∼Ub), wherein the C-terminus of Ub lies sandwiched between the loop containing the active site cysteine, Ubc13∼Ub also predominantly adopts a catalytically "inactive" conformation for which the C-terminus of Ub is outside of the active site.[29−31] Therefore, we conducted simulations for wild type and A122G-Ubc13∼Ub in the catalytically inactive conformation and analyzed the gating rates as described above for the active conformation, with the exception that the opening and closing kinetics for the gate were calculated by analyzing the stochastic fluctuations of the distance between the center of mass for the main chain N, Cα, C′ atoms from residues 119−121 of the gating loop and a fixed point in the hydrophobic core of the protein given by the center of mass for the main chain N, Cα, C′ atoms from residues V69, I108, with a distance cutoff of 15.5 Å. The choice for this general distance differs from that for the closed and catalytically active state, as the C-terminus of Ub tends to drag the loop containing the active site cysteine in the open state. This is a result of Ub not being as closely associated with Ubc13 as it is in the closed and catalytically active state. These simulations indicate that the gating rates for the catalytically inactive conformation of Ubc13∼Ub are similar to those for free Ubc13. Therefore, we have used the gating rates for free Ubc13 in the kinetic scheme employed to analyze enzyme kinetics, as described in detail below. It should be noted that simulations for the catalytically inactive state are more challenging to conduct than those for the catalytically active state, as a result of Ub extending out from Ubc13; this results in the requirement for larger solvation boxes, and difficulty for Ub to fully sample conformational space with respect to Ubc13.

Hydrolysis Assays. E1 enzyme and acceptor Ub were purchased from Boston Biochem, (Cambridge, MA). The kinetics of Ubc13∼Ub thioester hydrolysis were characterized with SDS-PAGE and using donor Ub site-specifically labeled with AlexaFluor488 as previously described.[9] Ubc13 or stochastic gate mutants (D118G, L121G, A122G) were conjugated to the C-terminus of Ub using 0.15 μM E1 (0.21 and 0.54 μM for A122G and L121G, respectively) in the presence of 3 mM ATP, 3 mM Mg^{2+}, 9.5 μM AlexaFluor488-labeled acceptor Ub, and 10 μM E2 for 60−90 min. The E1 was inactivated by adding 150 μM PYR-41 and waiting 30 min.[32] The loss of E2∼Ub thioester conjugate due to hydrolysis was then followed by the collection of 5−6 5 μL aliquots over ∼120−150 min. Aliquots were loaded onto SDS-PAGE gels and visualized using fluorescence at 517 nm with a Typhoon 9400 Imager. The fraction of Ubc13 conjugated to Ub was assessed with SYPRO Ruby total protein stain after fluorescent imaging of gels. The loss of E2∼Ub thioester and buildup of Ub were fit to two parameter exponential decay or growth, respectively, to yield the first order rate constant for hydrolysis.

Lysine Aminolysis Assays. The kinetics of Ubc13∼Ub thioester aminolysis by lysine were characterized by charging E2 with Ub as described for hydrolysis assays for wild type Ubc13, and the D118G, L121G, and A122G mutants. Following E1 inactivation by PYR-41, the loss of E2∼Ub thioester conjugate and the concomitant buildup of Ub resulting from the addition of lysine were followed by collection of 5−6 5 μL aliquots over ∼60 min. Lysine concentrations ranged from ∼10−100 mM. Reaction aliquots were imaged as described above for hydrolysis. The loss of E2∼Ub thioester and buildup of Ub were fit to two parameter exponential decay or growth, respectively, to yield a first order rate constant for aminolysis. The observed rate of aminolysis was quadratic with respect to lysine concentration, indicating that the reaction is described by

$$\frac{d[\text{E2}\sim\text{Ub}]}{dt} = -k_{cat,1}[\text{lys}^0][\text{E2}\sim\text{Ub}] - k_{cat,2}[\text{lys}^0][\text{lys}^0][\text{E2}\sim\text{Ub}] \quad (2)$$

where lys^0 indicates lysine with the side chain in the neutral state. Thus, plots of $k_{obs}/[\text{lys}^0]$ as a function of $[\text{lys}^0]$ result in straight lines that yield the rate constants ($k_{cat,1}$ and $k_{cat,2}$) for the overall aminolysis reaction. The first term in eq 2 is derived on the basis that only the neutral form ($-NH_2$) of the lysine side chain is capable of nucleophilic attack on the carbonyl carbon of the E2∼Ub thioester bond. The

$$
\begin{aligned}
\frac{d[\mathrm{Ub}]}{dt} &= k_{\mathrm{H_2O}}[\mathrm{E2_{OAnb}}\sim\mathrm{Ub}] + k_{\mathrm{H_2O}}[\mathrm{E2_{OAb}}\sim\mathrm{Ub}] \\
\frac{d[\mathrm{lys^0}]}{dt} &= -k_{\mathrm{cat,1}}[\mathrm{E2_{CAb}}\sim\mathrm{Ub}][\mathrm{lys^0}] - k_{\mathrm{cat,2}}[\mathrm{E2_{CAb}}\sim\mathrm{Ub}][\mathrm{lys^0}][\mathrm{lys^0}] \\
\frac{d[\mathrm{E2}]}{dt} &= k_{\mathrm{H_2O}}[\mathrm{E2_{OAnb}}\sim\mathrm{Ub}] + k_{\mathrm{H_2O}}[\mathrm{E2_{OAb}}\sim\mathrm{Ub}] + k_{\mathrm{cat,1}}[\mathrm{E2_{CAb}}\sim\mathrm{Ub}][\mathrm{lys^0}] + k_{\mathrm{cat,2}}[\mathrm{E2_{CAb}}\sim\mathrm{Ub}][\mathrm{lys^0}][\mathrm{lys^0}] \\
\frac{d[\mathrm{lys^0}\sim\mathrm{Ub}]}{dt} &= k_{\mathrm{cat,1}}[\mathrm{E2_{CAb}}\sim\mathrm{Ub}][\mathrm{lys^0}] + k_{\mathrm{cat,2}}[\mathrm{E2_{CAb}}\sim\mathrm{Ub}][\mathrm{lys^0}][\mathrm{lys^0}] \\
\frac{d[\mathrm{E2_{OAb}}\sim\mathrm{Ub}]}{dt} &= -k_{\mathrm{H_2O}}[\mathrm{E2_{OAb}}\sim\mathrm{Ub}] - k_{\mathrm{close,1}}[\mathrm{E2_{OAb}}\sim\mathrm{Ub}] + k_{\mathrm{open,1}}[\mathrm{E2_{CAb}}\sim\mathrm{Ub}] \\
&\quad - k_{\mathrm{close,2}}[\mathrm{E2_{OAb}}\sim\mathrm{Ub}][\mathrm{lys^0}] + k_{\mathrm{open,2}}[\mathrm{E2_{CAb}}\sim\mathrm{Ub}][\mathrm{lys^0}] \\
&\quad - k_{\mathrm{close,2}}[\mathrm{E2_{OAb}}\sim\mathrm{Ub}][\mathrm{lys^0}][\mathrm{lys^0}] + k_{\mathrm{open,2}}[\mathrm{E2_{CAb}}\sim\mathrm{Ub}][\mathrm{lys^0}][\mathrm{lys^0}] \\
&\quad + k_{\mathrm{bm}}[\mathrm{E2_{OAnb}}\sim\mathrm{Ub}] - k_{\mathrm{bb}}[\mathrm{E2_{OAb}}\sim\mathrm{Ub}] \\
&\quad + k_{\mathrm{bm}}[\mathrm{E2_{OAnb}}\sim\mathrm{Ub}][\mathrm{lys^0}] - k_{\mathrm{bb}}[\mathrm{E2_{OAb}}\sim\mathrm{Ub}][\mathrm{lys^0}] \\
&\quad + k_{\mathrm{bm}}[\mathrm{E2_{OAnb}}\sim\mathrm{Ub}][\mathrm{lys^0}][\mathrm{lys^0}] - k_{\mathrm{bb}}[\mathrm{E2_{OAb}}\sim\mathrm{Ub}][\mathrm{lys^0}][\mathrm{lys^0}] \\
\frac{d[\mathrm{E2_{CAb}}\sim\mathrm{Ub}]}{dt} &= -k_{\mathrm{cat,1}}[\mathrm{E2_{CAb}}\sim\mathrm{Ub}][\mathrm{lys^0}] - k_{\mathrm{cat,1}}[\mathrm{E2_{CAb}}\sim\mathrm{Ub}][\mathrm{lys^0}][\mathrm{lys^0}] \\
&\quad - k_{\mathrm{bb}}[\mathrm{E2_{CAb}}\sim\mathrm{Ub}] + k_{\mathrm{bm}}[\mathrm{E2_{CAnb}}\sim\mathrm{Ub}] + k_{\mathrm{close,1}}[\mathrm{E2_{OAb}}\sim\mathrm{Ub}] - k_{\mathrm{open,1}}[\mathrm{E2_{CAb}}\sim\mathrm{Ub}] \\
&\quad - k_{\mathrm{bb}}[\mathrm{E2_{CAb}}\sim\mathrm{Ub}][\mathrm{lys^0}] + k_{\mathrm{bm}}[\mathrm{E2_{CAnb}}\sim\mathrm{Ub}][\mathrm{lys^0}] \\
&\quad + k_{\mathrm{close,2}}[\mathrm{E2_{OAb}}\sim\mathrm{Ub}][\mathrm{lys^0}] - k_{\mathrm{open,2}}[\mathrm{E2_{CAb}}\sim\mathrm{Ub}][\mathrm{lys^0}] \\
&\quad - k_{bb}[\mathrm{E2_{CAb}}\sim\mathrm{Ub}][\mathrm{lys^0}][\mathrm{lys^0}] + k_{\mathrm{bm}}[\mathrm{E2_{CAnb}}\sim\mathrm{Ub}][\mathrm{lys^0}][\mathrm{lys^0}] \\
&\quad + k_{\mathrm{close,2}}[\mathrm{E2_{OAb}}\sim\mathrm{Ub}][\mathrm{lys^0}][\mathrm{lys^0}] - k_{\mathrm{open,2}}[\mathrm{E2_{CAb}}\sim\mathrm{Ub}][\mathrm{lys^0}][\mathrm{lys^0}] \\
\frac{d[\mathrm{E2_{CAnb}}\sim\mathrm{Ub}]}{dt} &= k_{\mathrm{bb}}[\mathrm{E2_{CAb}}\sim\mathrm{Ub}] - k_{\mathrm{bm}}[\mathrm{E2_{CAnb}}\sim\mathrm{Ub}] + k_{\mathrm{close,1}}[\mathrm{E2_{OAnb}}\sim\mathrm{Ub}] - k_{\mathrm{open,1}}[\mathrm{E2_{CAnb}}\sim\mathrm{Ub}] \\
&\quad + k_{\mathrm{bb}}[\mathrm{E2_{CAb}}\sim\mathrm{Ub}][\mathrm{lys^0}] - k_{\mathrm{bm}}[\mathrm{E2_{CAnb}}\sim\mathrm{Ub}][\mathrm{lys^0}] \\
&\quad + k_{\mathrm{close,2}}[\mathrm{E2_{OAnb}}\sim\mathrm{Ub}][\mathrm{lys^0}] - k_{\mathrm{open,2}}[\mathrm{E2_{CAnb}}\sim\mathrm{Ub}][\mathrm{lys^0}] \\
&\quad + k_{\mathrm{bb}}[\mathrm{E2_{CAb}}\sim\mathrm{Ub}][\mathrm{lys^0}][\mathrm{lys^0}] - k_{\mathrm{bm}}[\mathrm{E2_{CAnb}}\sim\mathrm{Ub}][\mathrm{lys^0}][\mathrm{lys^0}] \\
&\quad + k_{\mathrm{close,2}}[\mathrm{E2_{OAnb}}\sim\mathrm{Ub}][\mathrm{lys^0}][\mathrm{lys^0}] - k_{\mathrm{open,2}}[\mathrm{E2_{CAnb}}\sim\mathrm{Ub}][\mathrm{lys^0}][\mathrm{lys^0}] \\
\frac{d[\mathrm{E2_{OAnb}}\sim\mathrm{Ub}]}{dt} &= -k_{\mathrm{H_2O}}[\mathrm{E2_{OAnb}}\sim\mathrm{Ub}] + k_{\mathrm{bb}}[\mathrm{E2_{OAb}}\sim\mathrm{Ub}] - k_{\mathrm{bm}}[\mathrm{E2_{OAnb}}\sim\mathrm{Ub}] \\
&\quad + k_{\mathrm{on}}[\mathrm{E2_O}\sim\mathrm{Ub}] - k_{\mathrm{off}}[\mathrm{E2_{OAnb}}\sim\mathrm{Ub}] + k_{\mathrm{on}}[\mathrm{E2_O}\sim\mathrm{Ub}][\mathrm{lys^0}] - k_{\mathrm{off}}[\mathrm{E2_{OAnb}}\sim\mathrm{Ub}][\mathrm{lys^0}] \\
&\quad + k_{\mathrm{on}}[\mathrm{E2_O}\sim\mathrm{Ub}][\mathrm{lys^0}][\mathrm{lys^0}] - k_{\mathrm{off}}[\mathrm{E2_{OAnb}}\sim\mathrm{Ub}][\mathrm{lys^0}][\mathrm{lys^0}] \\
&\quad - k_{\mathrm{close,1}}[\mathrm{E2_{OAnb}}\sim\mathrm{Ub}] + k_{\mathrm{open,1}}[\mathrm{E2_{CAnb}}\sim\mathrm{Ub}] \\
&\quad + k_{\mathrm{bb}}[\mathrm{E2_{OAb}}\sim\mathrm{Ub}][\mathrm{lys^0}] - k_{\mathrm{bm}}[\mathrm{E2_{OAnb}}\sim\mathrm{Ub}][\mathrm{lys^0}] \\
&\quad - k_{\mathrm{close,1}}[\mathrm{E2_{OAnb}}\sim\mathrm{Ub}][\mathrm{lys^0}] + k_{\mathrm{open,1}}[\mathrm{E2_{CAnb}}\sim\mathrm{Ub}][\mathrm{lys^0}] \\
&\quad + k_{\mathrm{bb}}[\mathrm{E2_{OAb}}\sim\mathrm{Ub}][\mathrm{lys^0}][\mathrm{lys^0}] - k_{\mathrm{bm}}[\mathrm{E2_{OAnb}}\sim\mathrm{Ub}][\mathrm{lys^0}][\mathrm{lys^0}] \\
&\quad - k_{\mathrm{close,1}}[\mathrm{E2_{OAnb}}\sim\mathrm{Ub}][\mathrm{lys^0}][\mathrm{lys^0}] + k_{\mathrm{open,1}}[\mathrm{E2_{CAnb}}\sim\mathrm{Ub}][\mathrm{lys^0}][\mathrm{lys^0}] \\
\frac{d[\mathrm{E2_O}\sim\mathrm{Ub}]}{dt} &= -k_{\mathrm{on}}[\mathrm{E2_O}\sim\mathrm{Ub}] + k_{\mathrm{off}}[\mathrm{E2_{OAnb}}\sim\mathrm{Ub}] - k_{\mathrm{close,1}}[\mathrm{E2_O}\sim\mathrm{Ub}] + k_{\mathrm{open,1}}[\mathrm{E2_C}\sim\mathrm{Ub}] \\
\frac{d[\mathrm{E2_C}\sim\mathrm{Ub}]}{dt} &= k_{\mathrm{close,1}}[\mathrm{E2_O}\sim\mathrm{Ub}] - k_{\mathrm{open,1}}[\mathrm{E2_C}\sim\mathrm{Ub}]
\end{aligned}
\tag{3}
$$

second term in eq 2 accounts for the possibility that upon nucleophilic attack of a neutral lysine side chain, a second neutral lysine can act as a general base to facilitate deprotonation of the positively charged transition state, (see, for example, Figures 1 and 2 in ref 9). For the various lysine concentrations used, the lys^0 concentration was calculated according to eq 2 in ref 9. The observed aminolysis reaction kinetics were not corrected for hydrolysis, as the large concentrations of lysine employed in the assays give apparent rates well in excess of the rate of hydrolysis. To assess the role of active site desolvation by loop residue L121, aminolysis assays were also conducted for the Ubc13 mutants L121A, L121V, and L121I in a similar fashion, with the exception that a single concentration of 75 mM lysine was employed.

E1 Assays. The kinetics of E1-catalyzed activation of Ubc13 to generate the Ubc13∼Ub thioester conjugate were analyzed using a reaction mixture containing 0.08−0.7 μM E1, 3 mM ATP, 3 mM Mg^{2+}, 9.5 μM AlexaFluor488-labeled acceptor Ub, and ∼9 μM Ubc13 (wild type, D118G, L121G, and A122G). Additional details regarding concentrations of enzymes are given in Supporting Information, Table S1. The buildup of Ubc13∼Ub thioester conjugate was characterized by detection of the fluorescence of AlexaFluor488-labeled Ub at 517 nm with a Typhoon 9400 Imager, subsequent to separation of the reaction products using SDS-PAGE. The buildup of thioester was fit to a two-parameter exponential to extract observed rates (k_{obs}); typical results are shown in Supporting Information, Figure S3. To facilitate comparison of E1 charging rates between the D118G, L121G, and A122G mutants and wild type Ubc13 enzyme, k_{obs} was divided by the concentration of E1 enzyme used in the various reactions to yield an apparent second order rate constant (k_{app}, Supporting Information, Table S1).

Ubiquitination Assays. The kinetics for catalysis of the synthesis of K63-linked polyubiquitin chains were characterized as previously described,[9] with the exception that E1 enzyme was inactivated by adding 150 μM PYR-41 and waiting 30 min, rather than addition of 50 mM EDTA. Furthermore, Ubc13-D118G, L121G, and A122G were analyzed in addition to wild type Ubc13 (Supporting Information, Table S2). To test the role of active site desolvation by loop residue

dx.doi.org/10.1021/ja505440b | J. Am. Chem. Soc. 2014, 136, 17446−17458

L121, ubiquitination assays were also conducted for Ubc13-L121A, -L121V, and -L121I (Supporting Information, Table S2).

Lysine Assays: Kinetic Scheme and Rate Laws for Simultaneous Hydrolysis and Aminolysis. The rate laws for simultaneous hydrolysis and aminolysis by lysine are given by the coupled ordinary differential equations in eq 3, where $E2_{CA}$~Ub indicates E2~Ub thioester conjugate where the C-terminus of Ub is within the active site (catalytically active conformation), and the gate has closed to catalyze the reaction, $E2_{OA}$~Ub indicates that the C-terminus of Ub lies within the active site, but the gate is open. $E2_{O}$~Ub indicates that the C-terminus of Ub is outside of the active site (catalytically inactive conformation) and the gate is open. $E2_{C}$~Ub indicates that the C-terminus of Ub is outside of the active site, and the gate is closed. The subscripts "b" and "nb" indicate whether the carbonyl oxygen from the thioester is hydrogen bonded or not hydrogen bonded to the side chain amide of N79 from the active site of Ubc13, respectively, and lys^0 indicates lysine with the side chain in the neutral form. The second and third order rate constants for catalysis of aminolysis with lysine substrate are given by $k_{cat,1}$ and $k_{cat,2}$, respectively. The first order rate constant for hydrolysis of the E2~Ub thioester conjugate is given by k_{H_2O}. The rates of opening and closing for the stochastic gate when the C-terminus of Ub is outside the active site, in the inactive conformation, are given by $k_{open,1}$ and $k_{closed,1}$, respectively, whereas when the C-terminus of Ub is inside the active site, in the active conformation, these rates are given by $k_{open,2}$ and $k_{closed,2}$. The rate of binding, or entry, of the C-terminus to the active site of the covalently attached E2 when the gate is open, is given by k_{on} with the associated off-rate (k_{off}). The rate of hydrogen bond formation between the thioester carbonyl and the side chain amide of N79 from the active site is given by k_{bm}, whereas the rate of hydrogen bond breakage is given by k_{bb}. A schematic overview of the kinetic scheme (eq 3) is given in Figure S4.

A general scheme to assess the role of stochastic gating dynamics on the observed hydrolysis and simultaneous hydrolysis and aminolysis reaction rates is as follows: the rate equations are numerically integrated using experimental (k_{H_2O}, $k_{cat,1}$ and $k_{cat,2}$), MD-derived ($k_{open,1}$, $k_{open,2}$ and $k_{closed,1}$, $k_{closed,2}$), and estimated (k_{on} and k_{off}) rate constants, with protein and lysine concentrations similar to those used experimentally. Subsequently, the theoretical overall reaction rate for wild type is then determined by scaling of the overall rate to match the observed rate. The different rates of gate opening and closing between wild type Ubc13 and the various stochastic gate mutants, as determined from MD simulations, give different overall rates of thioester loss, and allow for comparison of gating dynamics between the different mutants and wild type. The specific details of this general methodology are described below.

For the on and off rates of covalently attached Ub onto the active site of Ubc13 when the gate is open, we assumed that k_{on} is diffusion limited with a value of 10^9 M^{-1} s^{-1}, and that the pseudo first order rate constant k'_{on} is given by (10^9 M^{-1} s^{-1}) × ρ, where ρ is the local concentration of Ub, assumed to be 3 mM, a reasonable value for the length of the flexible C-terminus from Ub (~4 residues).[33,34] A physically reasonable value for the off rate of Ub from the active site was determined with the following equation for the tethered dissociation constant, $K_{D,t} = (1 - f_c)/f_c$, where f_c is the fraction of Ub tethered to E2 that can be considered in a bound, or near bound state in the absence of specific interaction between the two proteins. The value of f_c was estimated by assuming that Ub diffuses freely within a half-sphere centered on the attachment point for the E2 enzyme (the active site Cys), and that ~5% of the volume of the half-sphere represents Ub conformations in bound or near-bound conformations. Finally, an estimate for the upper limit of the off rate is $k_{off} = k_{on}\rho K_{D,t} = 6 \times 10^7$ s^{-1}. Therefore, this approximation is tantamount to assuming that the untethered dissociation constant is 57 mM. Consistent with this assumption of weak binding, the average $^1H^N$ and ^{15}N chemical shift changes for Ubc13 are very small (2.3 ppb), with a maximum of ~10 ppb, upon addition of a 8-fold excess of Ub into 60 μM Ubc13 (Supporting Information, Figure S5). In addition, NMR and SAXS experiments indicate that the covalently attached Ub within E2~Ub thioester conjugates is flexible, with on and off rates on the cusp of fast and intermediate exchange on the NMR time scale.[29−31] It is physically reasonable to assume that k_{on} and k_{off} retain similar values in wild type Ubc13 and the various mutants, given that k_{on} is determined by the local concentration of Ub with respect to Ubc13, and k_{off} is determined by the nature of the interface between Ub and Ubc13, neither of which change substantively for any of the mutants with respect to wild type.

Theoretical rates of hydrolysis were calculated using the above kinetic scheme, with the exception that terms involving aminolysis are excluded. The first order rate of hydrolysis, k_{H_2O}, is set to the experimental value of 0.0014 min^{-1}, and scaled by a factor of 4.1, such that the calculated rate of loss of total thioester matched that experimental rate of loss for wild type Ubc13. This scale factor is necessary as the rates for gate opening and closing are not explicitly accounted for in the experimentally determined hydrolysis rates, and the rate approximations described above may differ from the true values. Additionally, the actual kinetic scheme may be different. The initial E2~Ub thioester concentration was 10 μM, with k_{open} and k_{closed} set to the values determined for wild type Ubc13. The opening and closing rates for the stochastic gate were subsequently changed to MD-derived values for the various mutants, and the rate of hydrolysis, relative to wild type Ubc13, was calculated.

To calculate the theoretical rates of concurrent aminolysis and hydrolysis, the above estimated k_{on} and k_{off} rates were used in the integrated equations of the kinetic scheme, as well as the scaled k_{H_2O} from the theoretical hydrolysis analysis. The rate constants $k_{cat,1}$ and $k_{cat,2}$ were set to the experimental values for wild type Ubc13, 9.0×10^{-6} M^{-1} s^{-1} and 2.2×10^7 M^{-2} s^{-1}, respectively. The initial estimate for k_{off} was lowered to 5×10^4 s^{-1} to achieve better agreement with the experimental data. It is worth noting that large variations for k_{on} and k_{off} (exceeding 10-fold, and in opposite directions) between wild type and the various mutants are required to potentially mask the relative theoretical kinetic differences that arise from MD-derived gating and hydrogen bonding rates. As discussed above, such large differences for k_{on} and k_{off} are physically unrealistic. The theoretical lysine-concentration dependent rates were fit as a function of the neutral lysine concentration, [lys^0], to extract theoretical $k_{cat,2}$ values. Subsequently, the opening and closing rates were changed according to the values obtained from MD simulations for the various stochastic gate mutants, to calculate the overall rate of aminolysis and hydrolysis in comparison to wild type enzyme. The theoretical $k_{cat,2}$ values were multiplied by a normalization constant (1.9) such that experimental and theoretical values for wild type were identical. As in the case of hydrolysis, this scale factor is necessary as the rates for gate opening and closing are not explicitly accounted for in the experimentally determined aminolysis rates, and the rate approximations described above may differ from the true values. Additionally, the actual kinetic scheme may be different. However, the two and 4-fold scale factors for aminolysis and hydrolysis, respectively, correspond to respective differences of 0.3 and 0.8 kcal/mol in the overall barrier heights of the reactions, in comparison to the experimental values. These relatively small differences indicate that the kinetic scheme and associated approximations are reasonable within a general benchmark of 1 kcal/mol. Finally, variations in the theoretical $k_{cat,2}$ and k_{H_2O} were determined by taking unique combination of pairs or quadruples of dependent rates obtained from individual MD simulations conducted in duplicate or triplicate. That is, for wild type, A122G, and L121G, there are 2 ($k_{open,1}$, $k_{closed,1}$) × 2 ($k_{open,2}$, $k_{closed,2}$, k_{bb}, k_{bm}), or four combinations, and 2 ($k_{open,1}$, $k_{closed,1}$) × 3 ($k_{open,2}$, $k_{closed,2}$, k_{bb}, k_{bm}), or six combinations for D118G, that were used to calculate multiple values for $k_{cat,2}$ and k_{H_2O}.

RESULTS

Structure and Dynamics of the Active Site Loop for Unconjugated Ubc13 and Mutants. The crystal structures of the D118G, L121G, and A122G loop mutants are similar to that of wild type enzyme, superimposing with backbone

RMSDs of 0.15, 0.23, and 0.43 Å, for L121G, D118G, and A122G, respectively (Figure 1a, Supporting Information, Figure

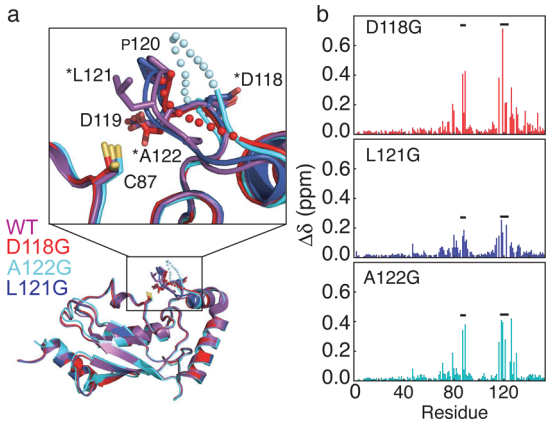

Figure 1. (a) Structures for Ubc13 and stochastic gate mutants, main chain regions with poor electron density are shown as spheres, gate residues mutated to glycine are indicated with an asterisk. (b) $^{15}N-^{1}H^{N}$ NMR chemical shift changes for stochastic gate mutants of Ubc13. Residues 87−89 and 118−122 are indicated with horizontal bars.

S6 and Table S3). The largest structural differences involve residues that comprise the stochastic gate (118−122). The nonhinge mutant L121G maintains a loop structure similar to wild type, whereas the hinge mutants D118G and A122G display different loop conformations with poorly defined electron density. These structural findings are also reflected in ^{15}N HSQC NMR spectra of the various mutants, which show significant chemical shift changes for residues within the stochastic gate, as well as the active site cysteine (Figure 1b). This latter finding highlights the intimate connection between the stochastic gate and residues where the covalent chemistry occurs. The smaller chemical shift changes in these regions for the L121G mutant in comparison to D118G and A122G are consistent with the similar structure of this mutant to wild type.

Differences in fast pico- to nanosecond time scale main chain dynamics for the mutants in comparison to wild type were assessed through measurement of ^{15}N-R_1, R_2, and NOE relaxation parameters (Figure 2 and Figure S7). The ^{15}N NMR relaxation parameters reveal that the stochastic gate is generally more flexible on the pico- to nanosecond time scale compared to surrounding regions of secondary structure for the wild type and mutant proteins (Figure S7). However, the gate for D118G and A122G mutants is more flexible than both the wild type and L121G proteins; this is evident in the results obtained from the NOE, a highly sensitive indicator for fast time scale flexibility of the protein main chain.

Enzyme Kinetics for Ubc13 and Stochastic Gate Mutants. The catalytic activity for wild type Ubc13 and the gate mutants was determined by measuring the rate of E2∼Ub thioester hydrolysis over a pH range from 7.0 to 8.5 (Figure 3a), as well as the rate of aminolysis of the thioester conjugate by lysine (Figure 3b). Overall, the rate of thioester hydrolysis catalyzed by D118G and A122G, Ubc13 mutants with more flexible stochastic gates, is increased in comparison to wild type and L121G. This result is consistent with the theoretically expected increase for reactions that are dependent solely on stochastic gate opening.[35,36] The rate constants for hydrolysis (k_{H_2O}) are weakly dependent upon pH, and range from ∼0.001

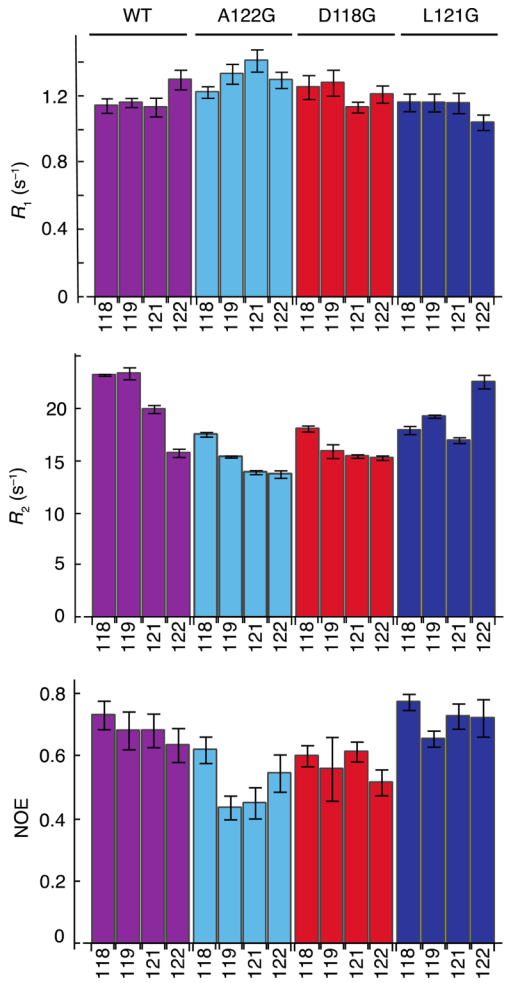

Figure 2. Main chain ^{15}N NMR relaxation parameters (600 MHz) for the stochastic gate from the E2 Ubc13 and gate mutants. For L121G, the contribution to R_2 from micro- to millisecond time scale dynamics (R_{ex}) was estimated as previously described[52] and subtracted from the experimental R_2 value.

to ∼0.003 min^{-1}. For the biological reaction, the rate of hydrolysis is catalyzed primarily by enzyme, whereas the associated reaction in water is catalyzed by hydroxide ion.[37] Thus, at physiological pH, the upper limit for the rate enhancement for hydrolysis achieved by the enzyme is ∼500-fold in comparison to the nonbiological catalyst, OH^-.[37] Interestingly, k_{app} for catalysis of the synthesis of E2∼Ub conjugates by E1 is ∼10^{11}-fold greater than that for hydrolysis of the thioester by water (Table S1 and Figure S3). Thus, for physiological concentrations of E1 and E2 (1−10 μM), the balance between E2 and E2∼Ub is shifted toward thioester as a result of the proficient catalytic activity of E1 enzyme.

For aminolysis of Ubc13∼Ub thioester by lysine, $k_{cat,2}$ ranges from (6.5 ± 0.1) × 10^6 M^{-2} s^{-1} for A122G and (1.9 ± 0.2) × 10^7 M^{-2} s^{-1} for D118G, to a maximum of (3.8 ± 0.3) × 10^7 M^{-2} s^{-1} for the wild type enzyme (Figure 3b). For L121G, aminolysis is severely impaired, with observed rates ∼200-fold slower than wild type. In water, $k_{cat,2}$ is ∼0.3 M^{-2} s^{-1} for aminolysis reactions of small molecule model compounds;[37] this 10^8 fold increase in the rate constant underscores the catalytic prowess of E2 enzymes; the cost of catalyzing biologically relevant aminolysis is paid for in large part by the structure and dynamics of the E2 enzyme.[9] Unlike hydrolysis,

dx.doi.org/10.1021/ja505440b | J. Am. Chem. Soc. 2014, 136, 17446−17458

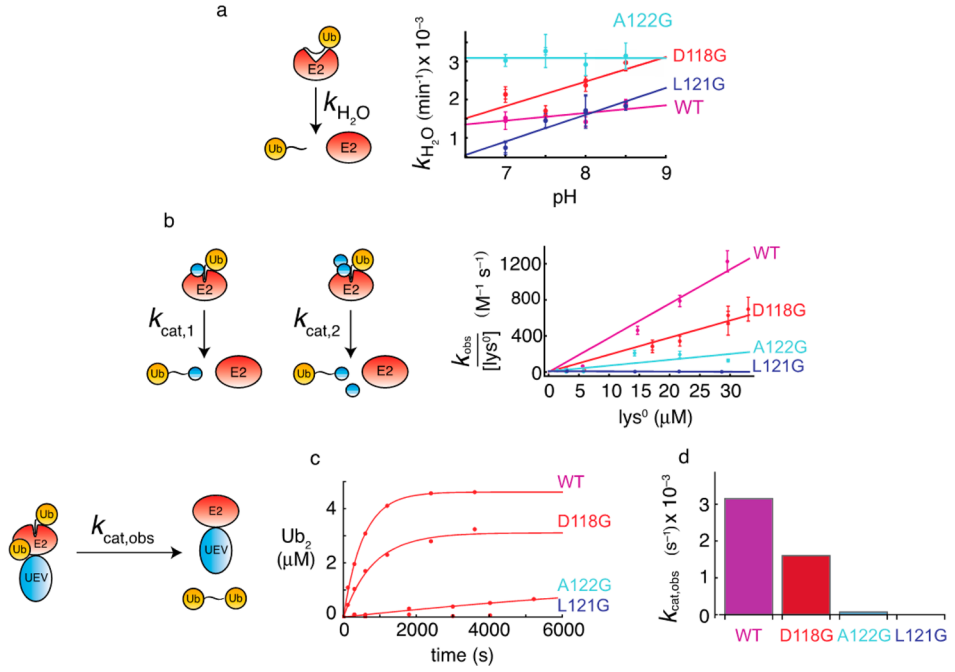

Figure 3. Kinetics of hydrolysis (a) and aminolysis (b) catalyzed by Ubc13 and stochastic gate mutants. In (b), neutral lysine (lys^0) is shown in blue. The straight lines in (b) represent fits of the data from which $k_{cat,1}$ and $k_{cat,2}$ were derived. (c) Catalysis of K63-linked Ub$_2$ chains by the heterodimer Mms2-Ubc13, and (d) fitted $k_{cat,obs}$ values (Supporting Information, Table S2). Mms2 is colored blue and labeled UEV.

catalysis of aminolysis is impaired to varying degrees for all Ubc13 mutants. For A122G, the observation that hydrolysis increases whereas aminolysis is impaired is consistent with the expected effect of gating on enzymatic reactions; that these rates change in opposite directions indicates that hydrolysis is dependent on opening, whereas aminolysis is dependent on closing.[35,36] Furthermore, addition of water to the thioester could be facilitated through a more open state, relative to the closed state, as water can act as a nucleophile and also as a catalyst by bridging the zwitterion. Specifically, the catalytic rate advantage for hydrolysis is ∼500-fold, extremely small in comparison to the 10^8-fold enhancement for aminolysis; this suggests that the small rate enhancement for hydrolysis is likely the result of modest solvation substitution effects combined with greater hydration for the open state at the active site surface of Ubc13. For mutants with more flexible gates, a decrease in the rate constant for aminolysis indicates that the rate of gate closure is diminished, as aminolysis by lysine likely requires the gate to close with concomitant desolvation to accomplish the chemical step. This is consistent with impaired aminolysis for L121G; loss of the hydrophobic side chain impairs desolvation of the active site, which is likely important for enhancing complementary electrostatic interactions between E2 enzyme and the transition state.[9] In order to test this hypothesis, we studied the kinetics of aminolysis for the mutants Ubc13-L121A, L121V, and L121I, in addition to L121G. This series of mutants possesses increasing hydrophobic accessible surface area (ASA) for their corresponding side chains; therefore, effects of desolvation should be linear as a function of hydrophobic ASA.[38] As shown in Figure 4a, there is an approximately linear increase in the rate of aminolysis with increasing hydrophobic ASA for the side chain of residue 121, consistent with a role for L121 in active site desolvation. However, given the similar hydrophobic surface areas for leucine and isoleucine side chains, the increased rate of aminolysis for wild type (L121), outside of the linear range,

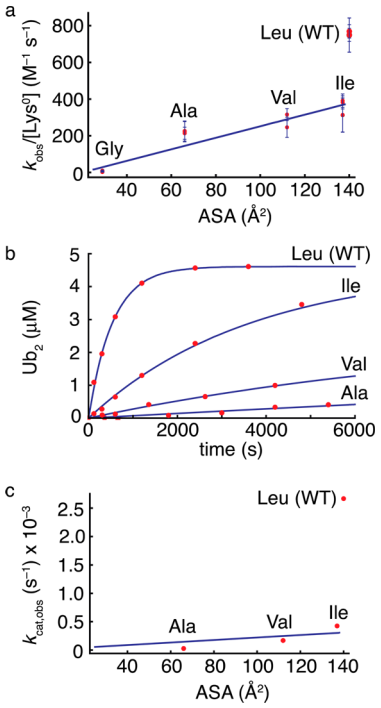

Figure 4. (a) Kinetics of aminolysis catalyzed by Ubc13-L121 mutants. (b) Catalysis of K63-linked Ub$_2$ chains by the heterodimer Mms2-Ubc13-L121 mutants, and (c) fitted $k_{cat,obs}$ values.

indicates that there are specific effects due to the nature of the side chain, and that Ubc13 is most efficient when leucine occupies this position.

In a biological context, Ubc13 catalyzes the synthesis of polyUb chains through tight association to Mms2, which positions Ub to react with Ubc13∼Ub.[18,39] Thus, we measured the rate of Ub$_2$ chain synthesis catalyzed by the holoenzyme

dx.doi.org/10.1021/ja505440b | J. Am. Chem. Soc. 2014, 136, 17446−17458

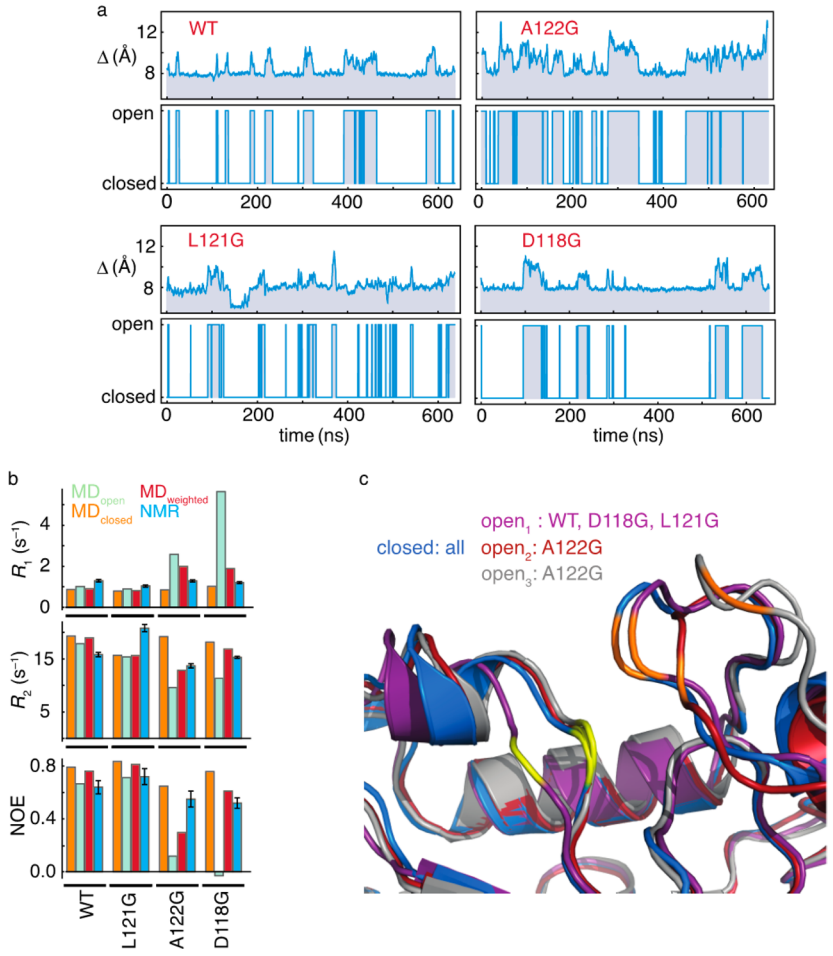

Figure 5. Stochastic gating for the active site loop of Ubc13 from MD simulations. (a) The distance (Δ) between the center of mass for residues 119−122 and that for residues 87−89 is shown in the upper panels. Digitization to a two state Markov process is shown in the lower panels. (b) Experimental and MD-derived ^{15}N NMR relaxation parameters for hinge residue 122 from Ubc13. For L121G, the contribution to R_2 from micro- to millisecond time scale dynamics (R_{ex}) was estimated as previously described[52] and subtracted from the experimental R_2 value. (c) Representative main chain structures from the closed and open states are shown; C87 is shown in yellow and L121 is shown in orange, the gate corresponds to residues 118−122.

(Figure 3c,d and Table S2). The results for the biologically relevant in vitro reaction are consistent with those for aminolysis. The 2-fold decrease in turnover rate for Ub_2 chain formation for D118G is the same as that for aminolysis, Ub_2 chain formation is defunct for L121G, and diminished for A122G. These results highlight a fundamental coupling between dynamics and structure for E2 enzymes; L121 plays a crucial structural role in the positioning of substrate lysine and concomitant active site desolvation, whereas the more open, dynamic active site for A122G reduces the fraction of time spent within a catalytically competent conformation. Desolvation effects for the holoenzyme are consistent with the results for aminolysis by lysine, with Ubc13-L121G, L121A, L121V, and L121I mutants showing a roughly linear increase in $k_{cat,obs}$ with increasing side chain hydrophobic surface area (Figure 4b,c and Table S2). Furthermore, specific effects due to the nature of the side chain are more pronounced for Ub_2 chain synthesis catalyzed by the holoenzyme, consistent with a crucial role for L121 in the positioning of substrate lysine.

MD Simulations Reveal Dynamic Differences for Ubc13 and Stochastic Gate Mutants. During MD simulations for unconjugated, or free Ubc13, the fluctuations of the gate as a function of time for Ubc13 and the various mutants are stochastic; thus, we derived rates assuming a two-state Markov chain (Figure 5). The rate of opening (k_{open}) varies from (3−12) × 10^7 s^{-1}, with k_{closed} ranging from (7−32) × 10^7 s^{-1} (Table 1). A122G stands out with the slowest closing rate, and an open state population of 64%, whereas the other mutants and wild type have open state populations of ∼20%. Representative structures for the open and closed states during the simulations are shown in Figure 5c, and highlight the conformational differences for the stochastic gate in the open and closed states. To assess whether the MD simulations represent experimental main chain dynamics, we calculated main chain ^{15}N R_1, R_2, and NOE relaxation parameters from the open and closed states for the various mutants and

Table 1. Stochastic Gating Rates and Populations Derived from ∼600 ns Time Scale MD Simulations for Unconjugated Ubc13

	closed:open	k_{open} × 10^7 (s^{-1})	k_{closed} × 10^7 (s^{-1})
WT	0.75:0.25	3.6	10.6
L121G	0.81:0.19	7.5	32.1
A122G	0.36:0.64	12.2	6.9
D118G	0.76:0.24	3.2	10.8

dx.doi.org/10.1021/ja505440b | J. Am. Chem. Soc. 2014, 136, 17446−17458

weighted these using their populations over the course of the simulations. The MD simulations capture the essential features of the main chain dynamics that are observed experimentally through measurements of ^{15}N R_1, R_2, and NOE relaxation parameters (Figure 5b). This was further validated for the most flexible mutants D118G and A122G, as their respective MD simulations produce significantly smaller RMSD values for experimental ^{15}N-R_1, R_2, and NOE values in comparison to the wild type simulation (Table S4). Importantly, the RMSD difference between the wild type simulation and that for A122G is five times greater than the sum of the experimental ^{15}N-R_1, R_2, and NOE errors for residues 118−122, or 10 times larger when considering only the most flexible residues (121 and 122). For D118G, the RMSD difference between the wild type simulation and D118G is also significant, two times greater than the sum of the experimental ^{15}N-R_1, R_2, and NOE errors for residues 118−122, or six times greater when considering only the most flexible residues (121 and 122). These results indicate that the respective MD simulations for A122G and D118G reproduce the respective experimental relaxation data to a significantly greater extent than the wild type MD simulation. Specifically, assuming that the experimental errors are normally distributed, the probabilities that the respective mutant simulations achieve better agreement than the wild type simulation by chance alone for residues 118−122 are 7×10^{-7} and 0.1 for A122G and D118G, respectively, and for residues 121−122, the probabilities are 1×10^{-23} and 7×10^{-10}, for A122G and D118G, respectively. The increased flexibility of the active site loop for A122G and D118G is a result of a more extensively populated open state with larger amplitude dynamics in comparison to the closed state (Figure 5). Complementary to these results, normalized *B*-factors determined from MD reflect trends observed for the crystal structures (Supporting Information, Figure S8). Given the differences in enzyme kinetics between wild type Ubc13 in the unconjugated state and the various stochastic gate mutants, the differences in dynamics observed experimentally and through MD suggest that dynamics may play a crucial role in the catalytic activity of ubiquitin conjugation enzymes.

To further explore the role of dynamics in E2 enzyme function, we conducted MD simulations for Ubc13 and the L121G, D118G, and A122G Ubc13 mutants conjugated to Ub through a thioester bond, in the catalytically active conformation wherein the C-terminus of Ub is within the enzyme active site (Figures 6 and 7). Typical structures for the open and closed states are shown in Figure 6b. The rate of opening varies from $\sim(2-5) \times 10^8$ s^{-1}, and k_{closed} ranges from $(1-9) \times 10^8$ s^{-1} (Table 2). As in the case of free Ubc13, gate fluctuations are stochastic, however, unlike free Ubc13, A122G and D118G populate closed conformations in the active state to a substantially greater extent than either wild type or L121G (Table 2). Interestingly, two closed conformations are observed in the MD simulations (Figure 6b). The second closed conformation ($L121_{closed,2}$) is substantially more populated for A122G- and D118G-Ubc13~Ub in the active conformation, in comparison to wild type. This closed conformation resembles that observed for the gating loops in a number of E2s other than Ubc13.

For the catalytically inactive Ubc13~Ub conjugate, MD simulations indicate that the gating rates for opening of wild type and A122G-Ubc13 thioester are similar to free Ubc13 within a ratio of 1.3 (free/thioester), and the gating rates for closing of wild type and A122G-Ubc13 are similar to free Ubc13 within a ratio of 0.5 (Figure S9). Thus, we used the gating rates for free Ubc13 for the catalytically inactive Ubc13~Ub thioester conjugate in the kinetic scheme described in detail below.

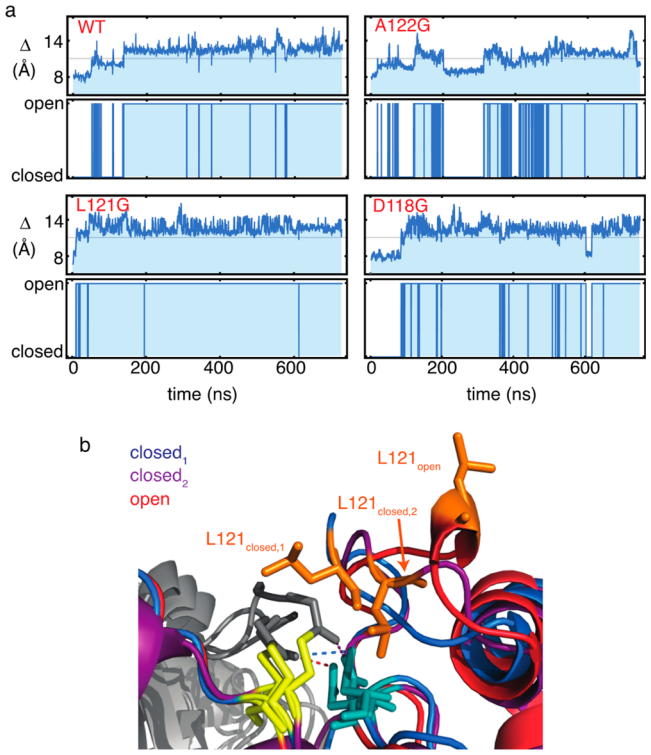

Figure 6. Stochastic gating for the active site loop of Ubc13 conjugated to Ub through a thioester bond from MD simulations. (a) The distance (Δ) between the center of mass for the main chain atoms from residues 121−122 and that for residue 87 is shown in the upper panels. Digitization to a two state Markov process is shown in the lower panels. (b) Representative main chain structures from the closed and open states are shown; C87 is shown in yellow, L121 is shown in orange, N79 is shown in teal, Ub is shown in gray, and hydrogen bonds between the thioester carbonyl and the side chain from N79 are shown as dashed lines; the gate corresponds to residues 118−122.

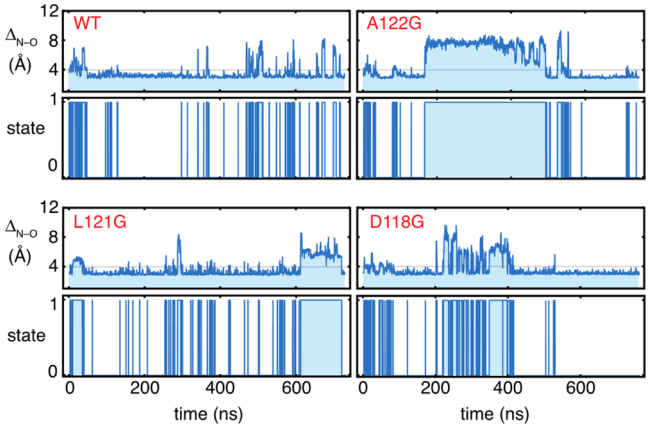

Figure 7. Stochastic fluctuations for the active site hydrogen bond between the thioester carbonyl carbon and N79 from Ubc13 from MD simulations. The distance between the carbonyl oxygen and the side chain amide nitrogen from N79 (Δ_{N-O}), is shown in the upper panels, and digitization to a two state Markov process is shown in the lower panels. State 0 is hydrogen bonded, whereas state 1 is not hydrogen bonded.

dx.doi.org/10.1021/ja505440b | J. Am. Chem. Soc. 2014, 136, 17446−17458

Table 2. Stochastic Gating Rates and Populations Derived from ~700 ns Time Scale MD Simulations for Ubc13~Ub in the Active Conformation

	closed:open	$k_{open} \times 10^8$ (s^{-1})	$k_{closed} \times 10^8$ (s^{-1})
WT	0.12:0.88	5.9	0.5
L121G	0.50:0.50	3.6	9.4
A122G	0.37:0.63	4.0	2.2
D118G	0.57:0.43	2.2	10.1

It would be ideal to compare MD simulations with ^{15}N NMR relaxation parameters for Ubc13 conjugated to Ub through a thioester bond. However, such experiments are compromised by slow hydrolysis (~2 h) of the thioester bond over the course of ^{15}N NMR relaxation measurements. Second, extensive line broadening of loop residues and the C-terminus of Ub, likely as a result of the entry of Ub into and out of the active site on the intermediate exchange time scale, renders ^{15}N NMR-based measurements difficult.[29,40] Nevertheless, the good agreement between ^{15}N NMR measurements and MD simulations for free Ubc13 suggest that the MD simulations for Ubc13~Ub are likely to faithfully capture the nature of the fast pico- to nanosecond time scale dynamics of the main chain.

It is curious that the observed decreases in the rates of aminolysis and ubiquitination for D118G- and A122G-Ubc13 are counterintuitive to the fact that these mutants have more populated closed states during MD simulations for the active Ubc13~Ub conformation. However, the mechanism of aminolysis and ubiquitination for E2 enzymes is thought to be dependent upon stabilization of the oxyanion transition state through hydrogen bonding to the side chain of N79 within the architecturally conserved active site HPN motif in E2 enzymes (Figure 6b).[41,42] Furthermore, two key theoretical concepts regarding the nature of enzyme catalysis are that the reaction barrier becomes small only when protein dynamics produce catalytically competent ground state configurations that lead to stabilization of the transition state, and that charge complementarity between a catalytically competent state in the enzyme and the transition state is crucial for catalysis.[43,44] Thus, we analyzed the rates of hydrogen bond formation and disruption between the side chain of N79 and the thioester carbonyl carbon (Table 3). The rate at which the hydrogen

Table 3. Active Site Stochastic Hydrogen Bonding Rates and Populations Derived from ~700 ns Time Scale MD Simulations for Ubc13~Ub in the Active Conformation

	bonded:not bonded	$k_{bb} \times 10^8$ (s^{-1})[a]	$k_{bm} \times 10^8$ (s^{-1})[b]
WT	0.87:0.13	1.1	7.6
L121G	0.62:0.38	2.1	3.3
A122G	0.35:0.65	1.7	0.8
D118G	0.64:0.36	1.0	6.2

[a] k_{bb} is the rate of hydrogen bond breaking. [b] k_{bm} is the rate of hydrogen bond making.

bond is made (k_{bm}) ranges from ~(1−8) × 10^8 s^{-1}, and the rate of bond breaking (k_{bb}) ranges from ~(1−2) × 10^8 s^{-1} (Table 3). The hydrogen bonded state for wild type Ubc13 is substantially more populated with a fraction bonded of ~0.9, in comparison to D118G, L121G, and A122G, with the latter mutant having a fraction bonded of ~0.4. Considering the importance of the active site hydrogen bond for the proposed stabilization of the transition state, the results for the status of this bond during MD simulations suggest that aminolysis, as well as catalysis of the synthesis of Ub_2 chains, will increase in the order A122G < L121G < D118G < WT. However, the overall catalytic rate will be balanced not only by the rate of hydrogen bond formation and breakage, but also by the rate of entry of C-terminus of Ub into the active site, as well as the gating rates when the C-terminus is within the active site, as discussed in detail below.

Coupling Rate Laws with MD Simulations Reveals the Role of Dynamics in Ubc13 Catalytic Activity. To develop a quantitative relationship between gating rates from MD simulations and observed enzyme kinetics, we derived the coupled ordinary differential equations, or rate laws, that describe the simultaneous hydrolysis and aminolysis catalyzed by E2 enzymes (eq 3). Using the rates of gating and active site hydrogen bonding for the HPN motif derived from MD simulations for the various mutants in the kinetic scheme allows for a critical assessment of the role of dynamics in the observed kinetics. Figure 8a shows that for the most dynamic stochastic

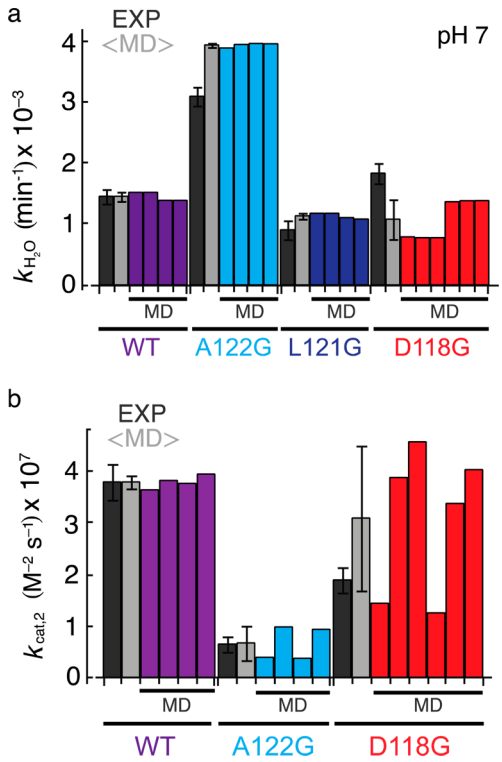

Figure 8. Coupling of kinetic rate laws with MD simulations. Experimental and MD-derived rates of hydrolysis (a) and aminolysis (b), catalyzed by the E2 Ubc13 and stochastic gate mutants.The multiple MD-derived $k_{cat,2}$ and k_{H_2O} rate constants were obtained by taking unique combinations of pairs of gating and hydrogen bonding rates derived from individual MD simulations, which were conducted in duplicate or triplicate.

gate mutant, A122G, the increased rate of gate opening determined from MD simulations quantitatively accounts for the increase in hydrolysis of the thioester conjugate at physiological pH. For L121G, the rate of gate closing for the active state of Ubc13~Ub is increased with respect to wild type, and is in excellent agreement with the decrease in the rate of hydrolysis observed for this mutant (Figure 8a). For D118G, the MD simulations slightly underestimate the relative rate of hydrolysis. This is a result of the increased population of the

dx.doi.org/10.1021/ja505440b | J. Am. Chem. Soc. 2014, 136, 17446−17458

second closed state ($L121_{closed,2}$ in Figure 6b) for the active conformation of the thioester conjugate. We have assumed that hydrolysis does not occur from either of the closed states; however, it is possible that it may occur from the second closed state, for which the thioester bond appears somewhat more exposed to solvent (Figure 6b).

An interesting feature of the kinetic scheme (eq 3) is that hydrolysis occurs from an open and activated state, that is, the C-terminus of ubiquitin is within the active site, and the gate is open. This explains the observation that A122G has an increased rate of hydrolysis and decreased rate of aminolysis compared to wild type enzyme; a direct consequence of the greater rate of opening. In contrast, the greater rate of gate closure for L121G is manifested as a decreased rate of hydrolysis.

Combining the gating rates from MD simulations with the kinetic rate laws illuminates the role of stochastic gate dynamics in regulating the rate of aminolysis by lysine (Figure 8b). When employed in conjunction with the kinetic rate laws, the increased rate of gate opening and less stable hydrogen bonding for the active site HPN motif for A122G, as determined from MD simulations, accurately predicts the experimental decrease in $k_{cat,2}$. For D118G, the decrease in $k_{cat,2}$ for the MD-derived value is correctly predicted, though somewhat overestimated, consistent with the results from hydrolysis. As in the case of hydrolysis, we assume that both closed states are equally effective for aminolysis (Figure 6b). However, it is possible that the second closed state is less effective at aminolysis, and this could potentially explain the modest overestimate of $k_{cat,2}$. With respect to free Ubc13, the overall agreement between experimental and MD-derived ^{15}N NMR relaxation parameters is good (Figure 5b), suggesting that the MD simulations for Ubc13~Ub and the various stochastic gate mutants are likely to correctly predict the dynamics for the thioester conjugated Ubc13 and mutants as well. Thus, the overall results for the kinetics of aminolysis, in combination with those for thioester hydrolysis, demonstrate that changes in fast pico- to nanosecond time scale main chain dynamics play a major role in determining the differences in kinetics between wild type Ubc13 and the various stochastic gate mutants. In general, opening and closing rates for enzyme active site gates occur on relatively slow time scales, in the millisecond to seconds range,[45,46] and are rate limiting with respect to k_{cat}. The fast, nanosecond time scale gating rates observed for Ubc13 are not rate limiting, rather, they play an important role in modulating k_{cat} as a function of the fraction of closed state and hydrogen bonded status of the architecturally conserved HPN motif. This view for the role of dynamics in enzyme catalysis is consistent with quantized molecular dynamics simulations, which indicate that large amplitude protein fluctuations are involved in gating the barrier for the intrinsic chemical reaction.[47]

It is interesting that the aminolysis rate constant $k_{cat,2}$ is greatly diminished for L121G, considering that catalysis should occur from within a closed and activated state, and therefore be at least similar to that of wild type. This finding sheds light on the role of the closed state from a structural perspective. The bulky, hydrophobic leucine side chain is likely to be crucial for achieving electrostatic enhancement of the chemical step through desolvation of the active site. Indeed, we observe an approximately linear increase in the rate of aminolysis and the synthesis of Ub_2 chains as a function of increasing hydrophobic surface area at position 121. Exclusion of water from the active site facilitates deprotonation of the substrate lysine amino group, and enhances the complementary electrostatic interactions between the active site and transition state.[9,48] However, given the substantial increase in the rates of aminolysis and Ub_2 synthesis for wild type Ubc13 in comparison to the L121I mutant, it is clear that the nature of the leucine side chain, which lacks a β-branch, plays an important role in determining specific effects as well.

Further indirect support that E2 enzymes have evolved to catalyze biologically relevant aminolysis by balancing structure with a flexibile stochastic gate that fluctuates between open and closed state, is evident in the structures of Mms2 and Uev1a, E2 ubiquitination enzyme variants that are unable to catalyze aminolysis.[15,19] Not only is the catalytic cysteine absent from the active site, the loop region is nonexistent, suggesting that in addition to a key structural role for loop residue D119 in stabilizing the transition state,[9] closure of the gate is indispensible for catalysis (Supporting Information, Figure S10). This is consistent with a model in which chemical factors directly involved in bond formation and breaking are important in the catalytic activity of enzymes, but that other factors, such as gating, also play a crucial role in catalysis.[49] Thus, there is potential for substantial residual catalytic activity, even if the catalytic cysteine is mutated; to completely abolish activity, multiple catalytic mechanisms must be disrupted, including, for example, gating mechanisms.

In Vivo Functional Complementation of the Yeast *ubc13* Gene by the Human Gene and Stochastic Gate Mutants. The ability of the human *UBC13* gene and its various stochastic gate mutants to rescue yeast *UBC13* deletion (*ubc13*Δ) mutants from lethal DNA damage by the methylating agent methylmethanesulfonate (MMS) is reflected in the ability of yeast to grow further along an MMS gradient on yeast extract peptone dextrose (YPD) plates. As shown in Figure 9,

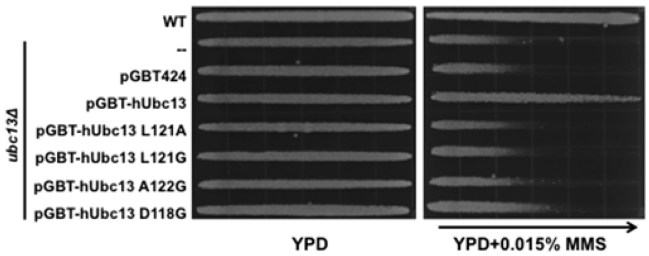

Figure 9. In vivo functional complementation of yeast Ubc13 with human Ubc13 and various stochastic gate mutants.

human *UBC13* can relieve the sensitivity of the yeast *ubc13*Δ mutant to MMS. In contrast, *ubc13*Δ cells carrying the corresponding human *ubc13*-L121G, -A122G, and -D118G mutations show a marked inability to grow in the MMS gradient plate. Furthermore, the ability of the *ubc13*-L121A mutant to tolerate MMS is also impaired, highlighting the importance of a bulky hydrophobic residue at position 121 in Ubc13.

DISCUSSION

Fast pico- to nanosecond time scale active site loop fluctuations play a crucial role in regulating the catalytic activity of ubiquitination enzymes. The stochastic gate mutants A122G and D118G have impaired function with respect to wild type; nevertheless, they possess catalytic rate enhancements in excess of ~10^7-fold. Thus, loop dynamics provide a thin layer of

regulation on top of a large catalytic advantage.[9] Yet, defects within this regulatory shell can have profound biological consequences, considering that Ubc13 is the only E2 dedicated to synthesizing Lys 63-linked polyUb chains. Ubc13-D118G and A122G show respective 2- and 40-fold reductions for the in vitro turnover rate ($k_{cat,obs}$) for attachment of the second Ub during synthesis of Lys 63-linked polyUb chains. While this appears modest for D118G, in vivo functional complementation assays reveal that both D118G and A122G demonstrate impaired defense against DNA damage resulting from exposure to the agent MMS (Figure 9). In addition, modest changes in the catalytic mechanism for D118G and A122G lead to 2 and 3-fold reductions in the apparent rate constant for activation of the E2 by E1 enzyme. These catalytic deficiencies are compounded to a greater extent in vivo than the impairment from changes in E2 active site loop dynamics suggests. This is likely a result of dependence of DNA repair on polyUb chain elongation,[50] and subsequent multivalent chain recognition;[34,51] each step in the sequential attachment of Ub during growth is impaired. Additionally, mutations may perturb overall E2 structure and stability, affecting interactions with Mms2 and Ub, and possibly E3 Ub ligases.

Different E2 enzymes catalyze the same chemical reaction, and are likely to rely on a stochastic gating mechanism. To adopt the conformation that stabilizes the transition state, the active site opens to allow entry of the C-terminus of Ub, and then closes to allow a structurally conserved Asp to stabilize the developing charge on the transition state. Furthermore, bulky hydrophobic residues such as L121 in Ubc13 are likely to play a role in desolvation of the active site to enhance electrostatic interactions, or solvation substitution,[48] though different residues may perform this function in disparate E2s. The β-hairpin and N-terminal region of the catalytic loop region appear structurally conserved in E2s, likely due to the catalytic requirement to position D119 close to the active site. However, the hinge region containing A122 in Ubc13, which involves the C-terminal region of the loop and the N-terminal region of helix α2, differs between Ubc13 and typical E2s such as UbcH5A.[13] These differences in the hinge region are likely related to specific binding and positioning of substrate lysine residues. Considering the importance of the hinge in dynamics of the loop region, it will be of great interest to explore the role of loop dynamics in regulating the catalytic activity of different E2 family members.

■ ASSOCIATED CONTENT

Supporting Information

Figures S1–S10, Tables S1–S4, and complete ref 25. This material is available free of charge via the Internet at http://pubs.acs.org.

■ AUTHOR INFORMATION

Corresponding Author

leo.spyracopoulos@ualberta.ca

Notes

The authors declare no competing financial interest.

■ ACKNOWLEDGMENTS

This research was supported by grants from the Canadian Institutes of Health Research (CIHR) to L.S. (MOP-110964) and W.X. (MOP-93612), and to J.N.M.G. from the Canadian Cancer Society. We thank the Canadian National High Field NMR Centre (NANUC) for assistance and use of the facilities. Operation of NANUC is funded in part by the University of Alberta. Computational studies were enabled by the use of computing resources provided by WestGrid and Compute/Calcul Canada. The coordinates for the structures of the Ubc13 mutants have been deposited in the Protein Data Bank (PDB accession codes 4NR3, 4NRG, 4NRI for L121G, D118G, and A122G, respectively).

■ REFERENCES

(1) Covert, M. W.; Leung, T. H.; Gaston, J. E.; Baltimore, D. *Science* **2005**, *309*, 1854.
(2) Petrini, J. H. J. *Science* **2007**, *316*, 1138.
(3) Jiang, X.; Chen, Z. J. *Nat. Rev. Immunol.* **2012**, *12*, 35.
(4) Wang, G.; Gao, Y.; Li, L.; Jin, G.; Cai, Z.; Chao, J. I.; Lin, H. K. *Front. Oncol.* **2012**, *2*, 5.
(5) Glickman, M. H.; Ciechanover, A. *Physiol. Rev.* **2002**, *82*, 373.
(6) Varshavsky, A. *Annu. Rev. Biochem.* **2012**, *81*, 167.
(7) Burroughs, A. M.; Jaffee, M.; Iyer, L. M.; Aravind, L. *J. Struct. Biol.* **2008**, *162*, 205.
(8) Ye, Y.; Rape, M. *Nat. Rev. Mol. Cell Biol.* **2009**, *10*, 755.
(9) Markin, C. J.; Saltibus, L. F.; Kean, M. J.; McKay, R. T.; Xiao, W.; Spyracopoulos, L. *J. Am. Chem. Soc.* **2010**, *132*, 17775.
(10) Ozkan, E.; Yu, H.; Deisenhofer, J. *Proc. Natl. Acad. Sci. U. S. A.* **2005**, *102*, 18890.
(11) Pierce, N. W.; Kleiger, G.; Shan, S. O.; Deshaies, R. J. *Nature* **2009**, *462*, 615.
(12) Pruneda, J. N.; Littlefield, P. J.; Soss, S. E.; Nordquist, K. A.; Chazin, W. J.; Brzovic, P. S.; Klevit, R. E. *Mol. Cell* **2012**, *47*, 933.
(13) Plechanovova, A.; Jaffray, E. G.; Tatham, M. H.; Naismith, J. H.; Hay, R. T. *Nature* **2012**, *489*, 115.
(14) Liu, Q.; Yuan, Y. C.; Shen, B.; Chen, D. J.; Chen, Y. *Biochemistry* **1999**, *38*, 1415.
(15) Moraes, T. F.; Edwards, R. A.; McKenna, S.; Pastushok, L.; Xiao, W.; Glover, J. N.; Ellison, M. J. *Nat. Struct. Biol.* **2001**, *8*, 669.
(16) Hofmann, R. M.; Pickart, C. M. *J. Biol. Chem.* **2001**, *276*, 27936.
(17) Marley, J.; Lu, M.; Bracken, C. *J. Biomol. NMR* **2001**, *20*, 71.
(18) Lewis, M. J.; Saltibus, L. F.; Hau, D. D.; Xiao, W.; Spyracopoulos, L. *J. Biomol. NMR* **2006**, *34*, 89.
(19) Hau, D. D.; Lewis, M. J.; Saltibus, L. F.; Pastushok, L.; Xiao, W.; Spyracopoulos, L. *Biochemistry* **2006**, *45*, 9866.
(20) Adams, P. D.; Afonine, P. V.; Bunkoczi, G.; Chen, V. B.; Davis, I. W.; Echols, N.; Headd, J. J.; Hung, L. W.; Kapral, G. J.; Grosse-Kunstleve, R. W.; McCoy, A. J.; Moriarty, N. W.; Oeffner, R.; Read, R. J.; Richardson, D. C.; Richardson, J. S.; Terwilliger, T. C.; Zwart, P. H. *Acta Crystallogr., Sect. D: Biol. Crystallogr.* **2010**, *66*, 213.
(21) Smith, D. K.; Radivojac, P.; Obradovic, Z.; Dunker, A. K.; Zhu, G. *Protein Sci.* **2003**, *12*, 1060.
(22) Farrow, N. A.; Muhandiram, R.; Singer, A. U.; Pascal, S. M.; Kay, C. M.; Gish, G.; Shoelson, S. E.; Pawson, T.; Forman-Kay, J. D.; Kay, L. E. *Biochemistry* **1994**, *33*, 5984.
(23) Kay, L. E.; Torchia, D. A.; Bax, A. *Biochemistry* **1989**, *28*, 8972.
(24) Spyracopoulos, L. *J. Biomol. NMR* **2006**, *36*, 215.
(25) Case, D. A. *AMBER 12*; University of California: San Fransico, 2012.
(26) Li, D. W.; Brüschweiler, R. *Angew. Chem., Int. Ed.* **2010**, *49*, 6778.
(27) Gotz, A. W.; Williamson, M. J.; Xu, D.; Poole, D.; Le Grand, S.; Walker, R. C. *J. Chem. Theory Comput.* **2012**, *8*, 1542.
(28) Showalter, S. A.; Brüschweiler, R. *J. Chem. Theory Comput.* **2007**, *3*, 961.
(29) McKenna, S.; Spyracopoulos, L.; Moraes, T.; Pastushok, L.; Ptak, C.; Xiao, W.; Ellison, M. J. *J. Biol. Chem.* **2001**, *276*, 40120.
(30) Pruneda, J. N.; Stoll, K. E.; Bolton, L. J.; Brzovic, P. S.; Klevit, R. E. *Biochemistry* **2011**, *50*, 1624.
(31) Soss, S. E.; Klevit, R. E.; Chazin, W. J. *Biochemistry* **2013**, *52*, 2991.

(32) Yang, Y.; Kitagaki, J.; Dai, R. M.; Tsai, Y. C.; Lorick, K. L.; Ludwig, R. L.; Pierre, S. A.; Jensen, J. P.; Davydov, I. V.; Oberoi, P.; Li, C. C.; Kenten, J. H.; Beutler, J. A.; Vousden, K. H.; Weissman, A. M. *Cancer Res.* **2007**, *67*, 9472.
(33) Zhou, H. X.; Gilson, M. K. *Chem. Rev.* **2009**, *109*, 4092.
(34) Markin, C. J.; Xiao, W.; Spyracopoulos, L. *J. Am. Chem. Soc.* **2010**, *132*, 11247.
(35) McCammon, J. A.; Northrup, S. H. *Nature* **1981**, *293*, 316.
(36) Szabo, A.; Shoup, D.; Northrup, S. H.; McCammon, J. A. *J. Chem. Phys.* **1982**, *77*, 4484.
(37) Connors, K. A.; Bender, M. L. *J. Org. Chem.* **1961**, *26*, 2498.
(38) König, G.; Bruckner, S.; Boresch, S. *Biophys. J.* **2013**, *104*, 453.
(39) Eddins, M. J.; Carlile, C. M.; Gomez, K. M.; Pickart, C. M.; Wolberger, C. *Nat. Struct. Mol. Biol.* **2006**, *13*, 915.
(40) McKenna, S.; Moraes, T.; Pastushok, L.; Ptak, C.; Xiao, W.; Spyracopoulos, L.; Ellison, M. J. *J. Biol. Chem.* **2003**, *278*, 13151.
(41) Wu, P. Y.; Hanlon, M.; Eddins, M.; Tsui, C.; Rogers, R. S.; Jensen, J. P.; Matunis, M. J.; Weissman, A. M.; Wolberger, C. P.; Pickart, C. M. *EMBO J.* **2003**, *22*, 5241.
(42) Cook, B. W.; Shaw, G. S. *Biochem. J.* **2012**, *445*, 167.
(43) Warshel, A. *Proc. Natl. Acad. Sci. U. S. A.* **1978**, *75*, 5250.
(44) Warshel, A. *Proc. Natl. Acad. Sci. U. S. A.* **1984**, *81*, 444.
(45) Religa, T. L.; Sprangers, R.; Kay, L. E. *Science* **2010**, *328*, 98.
(46) Whittier, S. K.; Hengge, A. C.; Loria, J. P. *Science* **2013**, *341*, 899.
(47) Boekelheide, N.; Salomon-Ferrer, R.; Miller, T. F. *Proc. Natl. Acad. Sci. U. S. A.* **2011**, *108*, 16159.
(48) Warshel, A.; Aqvist, J.; Creighton, S. *Proc. Natl. Acad. Sci. U. S. A.* **1989**, *86*, 5820.
(49) Wolfenden, R.; Snider, M. J. *Acc. Chem. Res.* **2001**, *34*, 938.
(50) Kim, H.; Chen, J. J.; Yu, X. H. *Science* **2007**, *316*, 1202.
(51) Sims, J. J.; Cohen, R. E. *Mol. Cell* **2009**, *33*, 775.
(52) Kneller, J. M.; Lu, M.; Bracken, C. *J. Am. Chem. Soc.* **2002**, *124*, 1852.